A 12-Port Circularly Polarized Dual-Band Back-Cover MIMO Antenna for 5G Smartphones

Asif Khan, Qingsha S. Cheng, *Senior Member, IEEE*, Yejun He, *Senior Member, IEEE*, Muhammad Zada, *Member, IEEE*, and Qingfeng Zhang, *Senior Member, IEEE*

***Abstract*—This letter presents a compact circularly polarized dual wide-bands twelve port multiple-input–multiple-output antenna for mobile terminal communications. It can be fitted into a smartphone as a back cover without occupying internal space. A single antenna module consists of a coaxial line feed port and a radiation patch with dimensions of $0.484\lambda_0 \times 0.591\lambda_0 \times 0.0203\lambda_0$ (where λ_0 is the free-space wavelength at 5 GHz). The measurement results indicate −6 dB bandwidths of 1.1 GHz (2.1 GHz to 3.2 GHz) and 0.5 GHz (5 GHz to 5.5 GHz), respectively. Significant isolation $\geq$ 18 dB, improved gain, and efficiency are achieved due to the introduction of the coronary stent-shaped-inspired metamaterial. The envelope correlation coefficient, the ratio of mean effective gains, and the efficiency are measured to be below 0.05, within 1 dB, and $\geq 90\%$, respectively. It also considers how the human hands impact the antenna's function. It operates over long-term evolution (LTE Band-1), LTE Band-40, worldwide interoperability for microwave access, LTE Band 41, NR Band n77, Wi-Fi 5 (802.11ac), Wi-Fi 6 (802.11ax), and NR Band n258.**

***Index Terms*—Coronary stent-shaped-inspired metamaterial (CSSIM), dual-band, multiple-input–multiple-output (MIMO) antenna, mutual coupling.**

I. Introduction

In RECENT years, significant progress has been made in the development of multiple-input–multiple-output (MIMO) antennas designed for 5G mobile phones [1]. These 5G MIMO antennas primarily operate in the sub-6 GHz frequency bands and are strategically positioned along mobile phones' longer edges or corners. In order to ensure compatibility with existing 2G, 3G, and 4G antennas, these antennas are typically located on the short edges of devices [2], [3]. Antennas mounted on the back cover of smartphones are considered better options than those installed on the edges or corners due to various limitations and the complexity of edge or corner designs [4], [11], [14], [15]. In [5], four short patches serve as radiators for an antenna pair covering the N79 band. Similarly, multiple narrow bands or wideband radiation have been achieved using half-mode patch antennas [6], [7], planar inverted-F antennas [8], [9], and slot antennas [10]. For advanced designs, characteristic mode analysis in [11] contributes to the development of a back-cover MIMO antenna with high isolation.

Circularly polarized (CP) MIMO antennas for terminal communication are uncommon but highly beneficial for modern communication. Since mobile devices, such as phones, are often used at varying angles, CP helps mitigate polarization mismatch and ensures stable communication regardless of device orientation. Most studies on terminal antennas feature linearly polarized designs with low gain and low efficiency [1], [7], [11], [14], [15]. Some designs use shared apertures, such as a three-port shared aperture antenna with CP mainly used for satellite communication [12] and a multiband monopole antenna with CP for GNSS applications [13]. However, these designs lack MIMO operation, wide bandwidth, and high gain.

This letter introduces a 12-element MIMO phone back-cover antenna based on a stitched pattern metamaterial, designed for 5G smartphones. The main innovation presented in this work is the integration of a novel CSSIM element to decrease mutual coupling, improve the gain and efficiency of the MIMO antenna, and achieve dual wide bands. To the best of the author's knowledge, this is the only 12-port MIMO antenna that operates across two wide frequency bands while exhibiting circular polarization.

II. Dual-Band Antenna and Metamaterial Designing

A. Operating Principle of the Proposed Design

A radiating patch printed on the top surface of Rogers AD255C dielectric substrate with a relative permittivity of 2.55 and loss tangent of 0.0015.

The iterative design process led us through various stages, given in Fig. 1(a). In Case-1, two resonating frequency bands are produced using an offset coaxial feed along the diagonal. The slots parallel to W_p (as in case-2) increase the resonating length. Therefore, a smaller value L_p will make it resonate at 3 GHz. In the following, the proposed stage (case-3) would have been kept similar and achieved the 2 GHz and 5 GHz bands is seen in Fig. 1(b). Basic physics involves altering the electromagnetic waves, extending the current path, decreasing intensity, and creating an additional resonating band by tuning their values. This process also supports the conversion of linear polarization to circular polarization, as shown in Fig. 1(c).

Received 11 February 2025; accepted 6 March 2025. Date of publication 11 March 2025; date of current version 9 July 2025. This work was supported in part by the National Natural Science Foundation of China under Grant 62071211; and in part by the Basic and Applied Basic Research Foundation of Guangdong Province under Grant 2021B1515120029. *(Corresponding author: Qingsha S. Cheng.)*

Asif Khan, Qingsha S. Cheng, and Qingfeng Zhang are with the Department of Electronic and Electrical Engineering, Southern University of Science and Technology, Shenzhen 518055, China (e-mail: asifm20019@gmail.com; chengqs@sustech.edu.cn; zhangqf@sustech.edu.cn).

Yejun He is with the College of Electronics and Information Engineering, Shenzhen University, Shenzhen 518060, China (e-mail: heyejun@126.com).

Muhammad Zada is with Biomedical and Mobile Health Technology Lab, Department of Health Sciences and Technology ETH Zürich, 8008 Zürich, Switzerland (e-mail: muhammad.zada@hest.ethz.ch).

Digital Object Identifier 10.1109/LAWP.2025.3549463

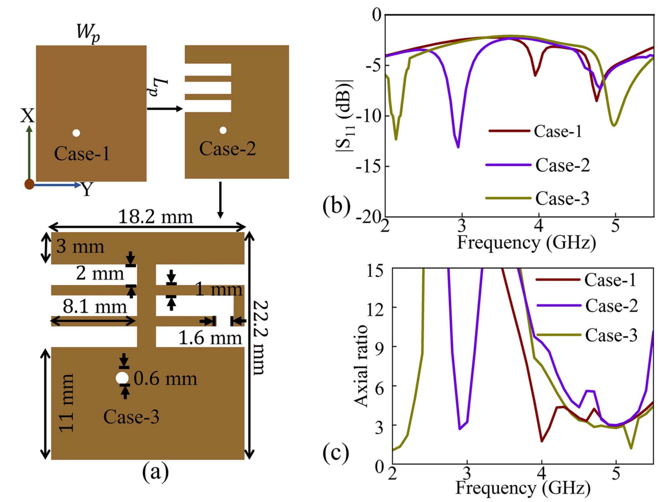

Fig. 1. (a) Iteration steps, (b) their reflection coefficients, and (c) axial ratio.

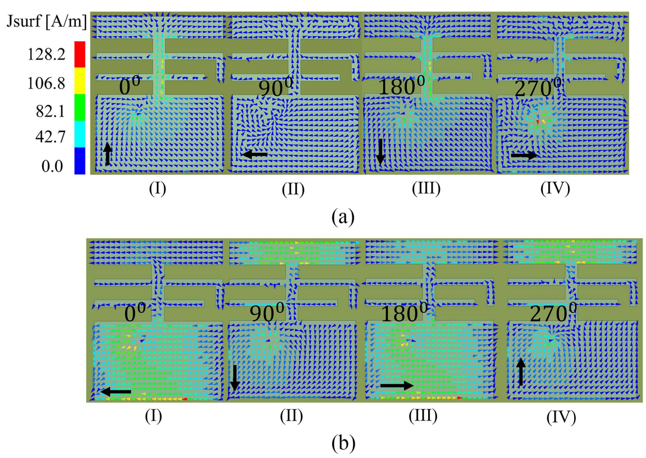

Fig. 2. Surface current distribution at various angles: (a) 2.5 GHz and (b) 5.3 GHz.

To demonstrate the implementation mechanism of circular polarization, Fig. 2(a) and (b) presents the surface current distribution of the antenna, as viewed from the +*Z*-axis, at four different phases (0°, 90°, 180°, and 270°) for the frequencies 2.5 GHz and 5.3 GHz, respectively. Arrows indicate the synthesized current direction.

At the 0° phase, the synthesized current direction predominantly aligns with the $-Y$-axis. At the 90° phase, it shifts to the *X*-axis. At the 180° phase, the current direction is mainly along the *Y*-axis, and at the 270° phase, it aligns with the $-X$-axis. The current amplitude remains equal but in opposite directions at phase pairs 0° and 180°, and 90°, and 270°. As the current rotates in an anticlockwise direction, the antenna successfully achieves right-hand circular polarization (RHCP) wave radiation across its bandwidths.

B. Coronary Stint-Shaped Inspired Metamaterial (CSSIM)

The proposed CSSIM, illustrated in Fig. 3(a), is designed to operate at 2.4 GHz to effectively reduce mutual coupling and enhance the gain of the MIMO antenna. The compact unit cell,

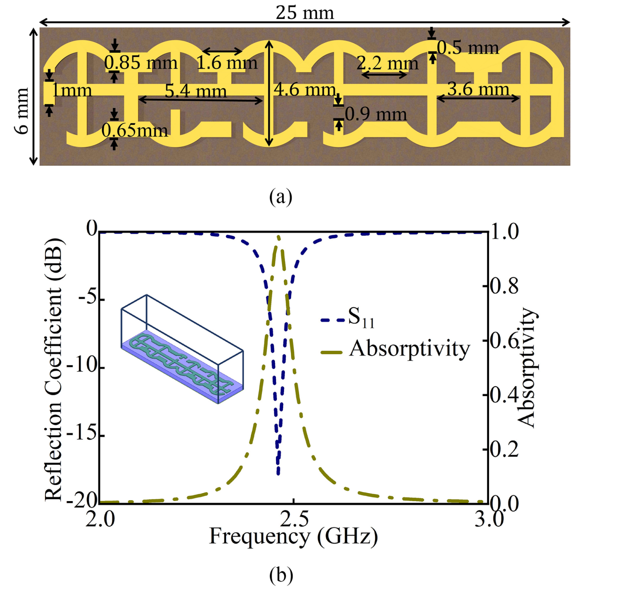

Fig. 3. (a) Schematic view of the CSSIM unit cell and (b) reflection coefficient and absorptivity.

with dimensions of $0.0798\lambda_0 \times 0.3325\lambda_0 \times 0.0101\lambda_0$, consists of interconnected semicircles linked by a strip with small branches at the center. This design leverages its metamaterial properties to achieve high absorption efficiency, high gain, and improved isolation performance. As shown in Fig. 3(b), the CSSIM exhibits strong absorption within the 2.4 GHz to 2.5 GHz range, achieving more than 80% absorptivity, as confirmed by the S_{11} and absorptivity plots. Optimized through a parametric study, the proposed absorber effectively suppresses unwanted radiation, minimizes mutual coupling, and enhances the radiation characteristics in the lower band.

III. Integration of the Single Antenna Into 12-Ports MIMO Antenna

A. S-Parameters

A 12 × 12 array MIMO antenna has been designed with an overall size of 150 mm × 75 mm × 0.762 mm, making it suitable for integration into the back of a mobile phone, as seen in Fig. 4(a) and (b). As the structure is symmetrical and complimentary in terms of placement, only ant-1, ant-2, and ant-12 are studied in this section, and the *S*-parameter results for ant-3 to ant-11 are excluded. Fig. 5(a) and (b) shows $S_{11,22\ 12-12}$ against the frequency. The proposed MIMO antenna achieves two wide bands: 2.1 GHz to 3.2 GHz and 5 GHz to 5.5 GHz. When antennas are placed together, mutual coupling between adjacent elements causes resonant modes to interact, effectively broadening the overall impedance bandwidth, as shown in Fig. 5(a).

The lower resonant band (LB) results from the offset coaxial feeding along the diagonal and the cuts in the patch. However, this modification leads to high mutual coupling, as well as reduced gain and efficiency between the antenna elements, particularly in the LB, as illustrated in Fig. 5(c). To address the challenge of high mutual coupling, two linear arrays of CSSIM

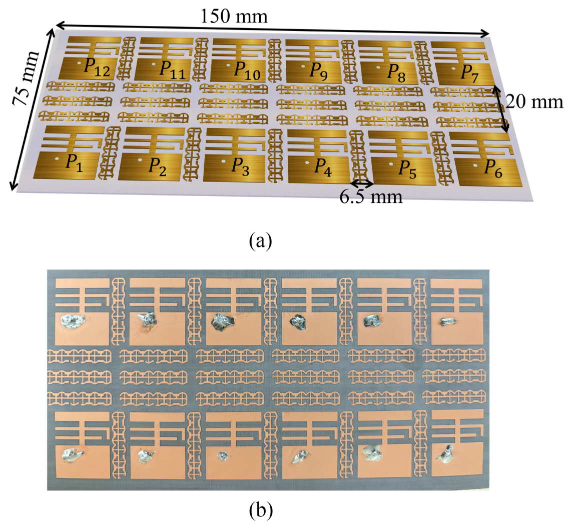

Fig. 4. (a) Schematic view of the proposed MIMO antenna. (b) Fabricated model of the proposed MIMO antenna.

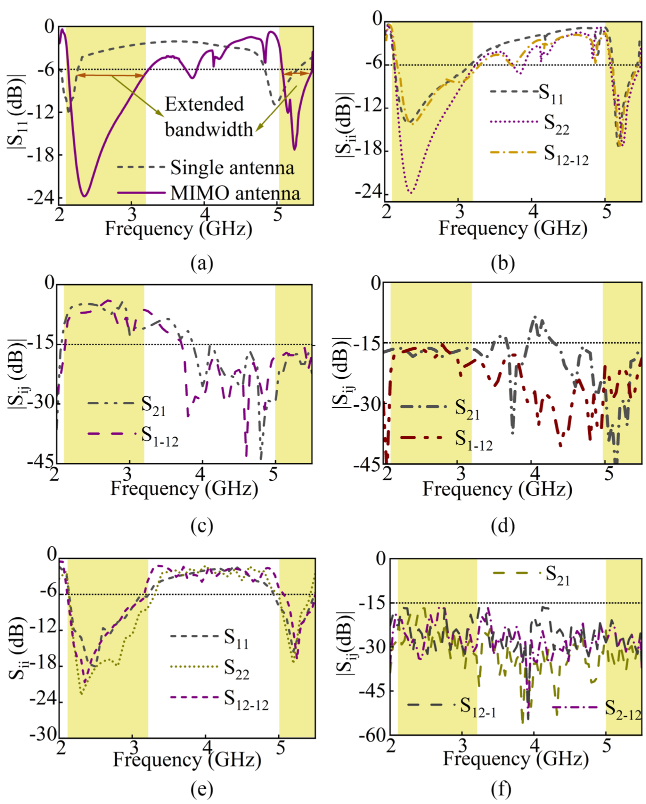

Fig. 5. *S*-parameters analysis (a) comparison of S_{ii} between a single antenna and the MIMO antenna; (b) S_{ii} of different ports of the MIMO antenna; (c) mutual coupling without CSSIM; (d) with CSSIM; (e) measured S_{ii}; and (f) S_{ij}.

are integrated along the *x*-plane and *y*-plane, significantly reducing mutual coupling to ≤ -18 dB, as illustrated in Fig. 5(d). The mutual decoupling is primarily attributed to the CSSIM arrays, which operate as absorbers, achieving 80% absorptivity in the LB and effectively mitigating unwanted electromagnetic

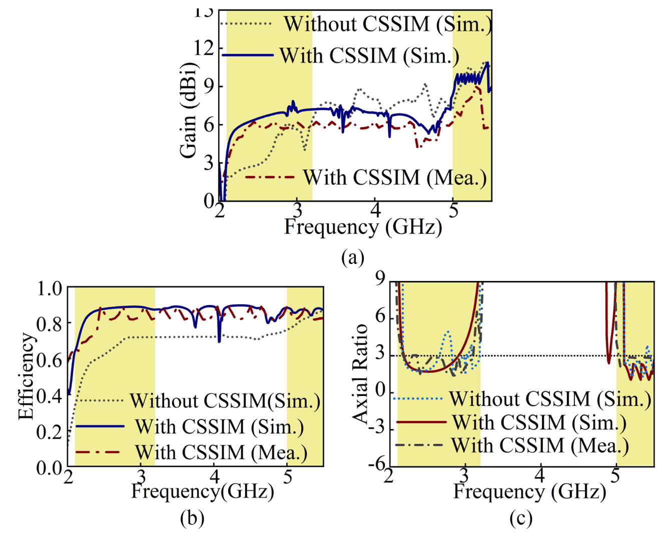

Fig. 6. Simulated and measured (a) gain, (b) efficiency, and (c) AR without and with CSSIM.

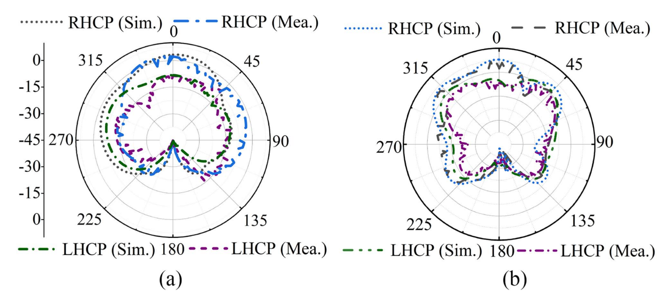

Fig. 7. LHCP and RHCP radiation patterns of the proposed MIMO antenna at (a) 2.4 GHz and (b) 5.3 GHz.

coupling between the antenna elements. The measured S_{ii} and S_{ij} are shown in Fig. 5(e) and (f). The simulated and measured data indicate impressive impedance matching, exceeding -6 dB in the 2.1 GHz to 3.2 GHz and 5 GHz to 5.5 GHz bands.

B. Radiation Performances

Gain and efficiency are critical performance metrics for mobile terminal antenna systems. In the LB, communication performance is limited due to the small patch antenna size. The integration of CSSIM arrays along the *X*- and *Y*-axes minimizes interference and improves radiation efficiency. This enhancement occurs through the suppression of surface waves and reduction of mutual coupling between adjacent antenna elements, leading to significant gain improvement. As a result, the gain increases from 2 dBi to 6 dBi, and the efficiency rises to 90%, as shown in Fig. 6(b) and (c), respectively. The simulated and measured axial ratios, presented in Fig. 6(d), cover an AR ≤ 3 dB bandwidth from 2.15 GHz to 3.1 GHz and 5.1 GHz to 5.5 GHz.

Fig. 7(a) and (b) presents the simulated and measured radiation patterns for left-hand circular polarization (LHCP) and RHCP at 2.4 GHz and 5.3 GHz, confirming the RHCP radiation at both frequencies. The CSSIM integration minimally impacts

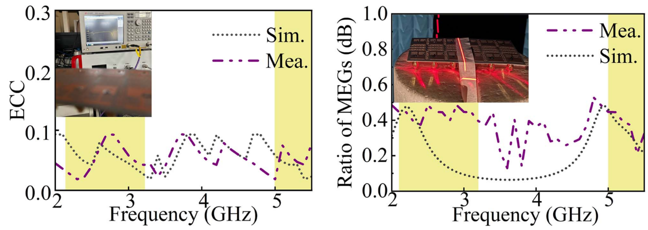

(a) (b)

Fig. 8. Simulated and measured MIMO diversity parameters: (a) ECC and (b) RMEGs.

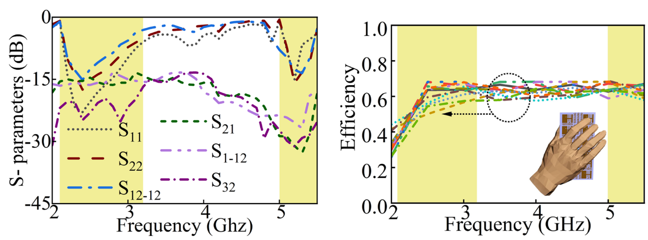

(a) (b)

Fig. 9. Representative application scenario of the SHM smartphone (a) *S*-parameters and (b) efficiencies of all antennas.

the radiation pattern, allowing the MIMO antenna to retain its original characteristics while reducing mutual coupling and improving gain.

C. MIMO Diversity Analysis

Fig. 8 presents the analysis of MIMO diversity for the 12 × 12 MIMO antenna, with ECC and RMGs determined using far–field measurements. As shown in Fig. 8(a) and (b), the simulated and measured ECCs and the ratios of MEGs are less than 0.1 dB and 0.8 dB in both bands, respectively, meeting the requirements of less than 0.5 for low correlation and less than 3 dB for comparable average received power [16]. Due to the structural symmetry, only the MIMO parameters of antenna-1 with respect to antenna-2 are measured. The measured ECCs and RMGs are well-matched to the simulated results.

D. Impact of User's Hand

When designing antennas for mobile phones, evaluating their performance in real-world usage scenarios is essential to ensure durability. Therefore, a thorough analysis is necessary to understand how the antenna, designed for smartphone integration, interacts with human tissue, ensuring its safe and effective operation.

Fig. 9(a) shows the corresponding *S*-parameters when single-hand mode (SHM) is utilized. Compared with the results shown in Fig. 5(b) and (d), the reflection coefficient and isolation of the antennas, with and without a hand, are similar. However, the efficiency of the suggested MIMO antenna is affected in SHM, as the hand is directly in contact with the antenna's elements, as shown in Fig. 9(b). The efficiency plot for the SHM case ranges from 50% to 70%, reflecting a 30% reduction compared to its performance in free space.

TABLE I
PERFORMANCE COMPARISON OF DIFFERENT BACK-COVER MIMO ANTENNAS

Ref.	[4]	[11]	[14]	[15]	This Work
BW (GHz)	4.4–5	3.3–3.8	3.3–5	3.4–4.3	2.1–3.2, 5–5.5
Gain (dBi)	6	NA	6	4.5	6.2, 9
Effi.	42	40	55-82	43	90, 90
Iso. (dB)	18	20	12	21	18
No of Elements	8	8	4	4	12
ECC	0.23	0.13	0.05	0.05	0.08, 0.05
RMEGs	1.96	0.13	NA	NA	0.6, 0.7
Pol.	LP	LP	LP	LP	CP

BW: Bandwidth, Effi.: Efficiency, Iso.: Isolation, ECC: Envelope Correlation Coefficient, RMEGs.: Ratio of mean effective gains Pol.: Polarization, LP: Linear polarization; CP: Circular Polarization.

IV. COMPARISON WITH OTHER TERMINAL ANTENNAS

Table I provides a comparative analysis of our recent research with other publications on back-cover MIMO antennas. Notably, our antenna design distinguishes itself primarily through its compact size for dual-band operation. It can be seen that all the recent works referenced, including [4], [11], [14], and [15], operate exclusively within a single frequency band. Similarly, the back cover MIMO antennas are either four-port [14], [15] or eight-port [4], [11]. However, in our case, the antenna is a 12-port design that covers the entire back area, similar to the designs in [4] and [14], which feature eight-port and four-port configurations, respectively.

In terms of gain, the proposed design achieves 6.2 dBi and 9 dBi, outperforming [4] and [14], which reported gains of 6 dBi and 4.5 dBi, respectively, while no gain data are provided for [11] and [15]. The efficiency of the proposed antenna is exceptionally high, reaching 90% in both bands, significantly exceeding the values reported in [4] (42%), [11] (40%), and [14] (55% to 82%). Ratio of mean effective gains (RMEGs) are also competitive, achieving 0.6 to 0.7, while the work in [4] and [11] report lower values (1.96 to 0.13).

A notable distinction is the polarization method, where the proposed design employs CP, offering improved multipath handling and polarization diversity. In contrast, all other designs utilize LP, which is less robust in multipath environments.

V. CONCLUSION

A CP dual-band, twelve-element MIMO antenna based on CSSIM is presented for 5 G mobile phones, with an analysis of its real-world applications. The antenna operates within measured −6 dB impedance bands of 2.1 GHz to 3.2 GHz and 5 GHz to 5.5 GHz. In particular, the MIMO antenna showcases mutual coupling ≤ -18 dB and ECCs below 0.05 across the bands. Remarkably, all elements of the proposed MIMO antenna maintain their efficiencies above 90% despite the substrate's 0.02 loss tangent and a low profile of just $0.02\lambda_0$. This study examines the design, operational methodology, parameter evaluations, and experimental results of the suggested MIMO antenna. Dual-band operation, compact structure, CP, high isolation, and high gain make this design ideal for next-generation 5G smartphones.

REFERENCES

[1] J. L. Guo, L. Cui, C. Li, and B. H. Sun, "Side-edge frame printed eight port dual-band antenna array for 5G smartphone applications," *IEEE Trans. Antennas Propag.*, vol. 66, no. 12, pp. 7412–7417, Dec. 2018.

[2] D. Huang, Z. Du, and Y. Wang, "An octa-band monopole antenna with a small nonground portion height for LTE/WLAN mobile phones," *IEEE Trans. Antennas Propag.*, vol. 65, no. 2, pp. 878–882, Feb. 2017.

[3] Y. Luo, Y. Liu, and S. Gong, "Nona-band antenna with small nonground portion for full-view display mobile phones," *IEEE Trans. Antennas Propag.*, vol. 68, no. 11, pp. 7624–7629, Nov. 2020.

[4] B. Cheng and Z. Du, "A wideband low-profile microstrip MIMO antenna for 5G mobile phones," *IEEE Trans. Antennas Propag.*, vol. 70, no. 2, pp. 1476–1481, Feb. 2022.

[5] B. Cheng and Z. Du, "Dual polarization MIMO antenna for 5G mobile phone applications," *IEEE Trans. Antennas Propag.*, vol. 69, no. 7, pp. 4160–4165, Jul. 2021.

[6] L. Chang, G. Zhang, and H. Wang, "Triple-band microstrip patch antenna and its four-antenna module based on half-mode patch for 5G 4×4 MIMO operation," *IEEE Trans. Antennas Propag.*, vol. 70, no. 1, pp. 67–74, Jan. 2022.

[7] K.-L. Wong, M.-F. Jian, and W.-Y. Li, "Low-profile wideband four corner-fed square patch antenna for 5G MIMO mobile antenna application," *IEEE Antennas Wireless Propag. Lett.*, vol. 20, no. 12, pp. 2554–2558, Dec. 2021.

[8] L. Chang and H. Wang, "Dual-band four-antenna module covering N78/N79 based on PIFA for 5G terminals," *IEEE Antennas Wireless Propag. Lett.*, vol. 21, no. 1, pp. 168–172, Jan. 2022.

[9] L. Chang and H. Wang, "Miniaturized wideband four-antenna module based on dual-mode PIFA for 5G 4×4 MIMO applications," *IEEE Trans. Antennas Propag.*, vol. 69, no. 9, pp. 5297–5304, Sep. 2021.

[10] I. R. R. Barani, K.-L. Wong, Y.-X. Zhang, and W.-Y. Li, "Low profile wideband conjoined open-slot antennas fed by grounded coplanar waveguides for 4×4 5G MIMO operation," *IEEE Trans. Antennas Propag.*, vol. 68, no. 4, pp. 2646–2657, Apr. 2020.

[11] W. Hu et al., "Wideband back-cover antenna design using dual characteristic modes with high isolation for 5G MIMO smartphone," *IEEE Trans. Antennas Propag.*, vol. 70, no. 7, pp. 5254–5265, Jul. 2022.

[12] S. Rao and Y. Wang, "Shared-aperture design of the cellular antenna and satellite communication antenna with circular polarization in S-band for metal-bezel smartphones," *IEEE Trans. Antennas Propag.*, vol. 72, no. 5, pp. 3938–3949, May 2024.

[13] Z. Liang, Y. Li, and Y. Long, "Multiband monopole mobile phone antenna with circular polarization for GNSS application," *IEEE Trans. Antennas Propag.*, vol. 62, no. 4, pp. 1910–1917, Apr. 2014.

[14] M. Hu and Y. Li, "Wideband back cover microstrip antenna with multiple shorting vias for mobile 5G MIMO applications," *IEEE Trans. Antennas Propag.*, vol. 71, no. 10, pp. 8290–8295, Oct. 2023.

[15] L. Qian, X. Chen, X. Liu, H. Zhou, H. Wang, and M. Hou, "Low-profile wideband patch antenna using even and odd modes for 5G terminal applications," *IEEE Antennas Wireless Propag. Lett.*, vol. 23, no. 8, pp. 2476–2480, Aug. 2024.

[16] Y. Ding, Z. Du, K. Gong, and Z. Feng, "A novel dual-band printed diversity antenna for mobile terminals," *IEEE Trans. Antennas Propag.*, vol. 55, no. 7, pp. 2088–2096, Jul. 2007.